



Variation of seismic amplitudes in the upper Macaé formation

Fabrcio O. Alves Augusto and Jorge Leonardo Martins

Coordenação da Área de Geofísica, Observatório Nacional - MCT, Brazil

Copyright 2009, SBGf - Sociedade Brasileira de Geofísica

This paper was prepared for presentation at the 11th International Congress of the Brazilian Geophysical Society, held in Salvador, Brazil, August 24-28, 2009.

Contents of this paper were reviewed by the Technical Committee of the 11th International Congress of The Brazilian Geophysical Society and do not necessarily represent any position of the SBGf, its officers or members. Electronic reproduction or storage of any part of this paper for commercial purposes without the written consent of The Brazilian Geophysical Society is prohibited.

Abstract

In this contribution, we study the seismic amplitude variation in the upper Macaé formation. This study is an important additional information in the characterization of mature reservoir as the Namorado reservoir. We constructed qualitative maps of normal-incidence seismic amplitudes in the Namorado oil field from geophysical logs. First, we calculated compressional-wave acoustic impedance from density and P-wave sonic logs, which is necessary information for calculating normal-incidence reflection coefficients. Then, we simulated seismic traces using convolution. Using estimators defined as inverse-weighted means in the interpolation process, we applied a variable search radius scheme for estimating seismic amplitudes in a given depth. The resulting map shows a concentration of negative seismic amplitudes in the W-E direction, suggesting the reservoir extension along the depth of 3103 m. The interpretation of such map may lead to the understanding of the evolution of areas in the reservoir with geological features favorable to the location of production or injection wells.

Introduction

Among the methods used in geophysical exploration for oil and gas about 95% are seismic methods. However, although they have high power of penetration and resolution, they must be integrated with other geophysical methods for minimizing the uncertainties in predictions. In general, geophysical well logging incorporates additional information in characterization procedures of oil and gas reservoirs (Dewan, 1983; Ellis, 1987), particularly in mature oil fields. For example, P-wave normal-incidence synthetic seismograms is the most common procedure to aid in the calibration of seismic amplitudes (Vidal et al., 2007).

Some Brazilian petroliferous field, as Namorado oil field, are in their mature stage. Typically, mature fields still have around 70% of the original volume of hydrocarbons inside the reservoir. Additional studies are necessary to slow down the decrease or even to increase oil production. In this way, maps of normal-incidence seismic amplitudes can be useful for monitoring reservoirs. These maps also help in the study the viability of 4D seismic surveys in mature

reservoirs, in order to increase oil and gas production. Additionally, integrated with other methodologies, these maps can be used, for example, to aid for evaluating fluid-injection connectivity between wells.

In this paper, we propose to construct maps of normal incidence seismic amplitude in the Namorado oil field, Campos basin, as in Augusto's (2009) dissertation. The objective is to analyze the extent of the reservoir at a given depth. We used variations of physical properties through the upper Macaé formation easily noticed at well surroundings by inspecting fundamental well logs. Nevertheless, the absence of P-wave sonic logs in most wells of the used data set prevents constructing normal-incidence synthetic seismograms. Therefore, we applied regression analysis methodology similar as in Han et al. (1986) and Miller and Stewart (1990) in order to predict P-wave sonic logs. Some of these regressions can be found in Augusto et al. (2007) and in Augusto and Martins (2008). These papers show multivariate linear and parabolic models for velocity prediction from fundamental petrophysical quantities, taking into account effective porosity, shaliness and electrical resistivity as the parameters of V_p dependence. Our methodology is described in the next section.

Methodology

The data set so called "Campo Escola Namorado" that contains information from nearly 50 wells drilled through the upper Macaé formation, where the oil-producing Namorado field is inserted (Tigre and Lucchesi, 1986). All wells contains fundamental geophysical logs, i.e., gamma ray (GR), resistivity (ILD), neutron porosity (NPHI), bulk density (RHOB) and P-wave sonic (DTP) logs, in the turbiditic interval between 2950 and 3150 m. However, we selected only wells in main block of the Namorado oil field, which totalized 39 wells as shows the Figure 1. Among this chosen wells, only 4 contains composite logs necessary to aid in the correlation of the results with the stratigraphic column. These wells are represented by red circles (see Figure 1). We apply the following steps for each wells in order to construct the resulting maps.

1 - Calculation of Acoustic Impedance

The product of density and velocity is defined as the acoustic impedance of the rock, i.e.,

$$I = \rho V_p \quad (1)$$

For the calculation of acoustic impedance log, ρ represents a reading in the bulk density log (g/cm^3) and V_p , the P-wave velocity in km/s converted from the sonic log ($\mu\text{s/ft}$). Note that we calculate acoustic impedance for compressional waves. Thus, the synthetic seismograms calculated below, to simulate normal incidence seismic data, are for P-waves.

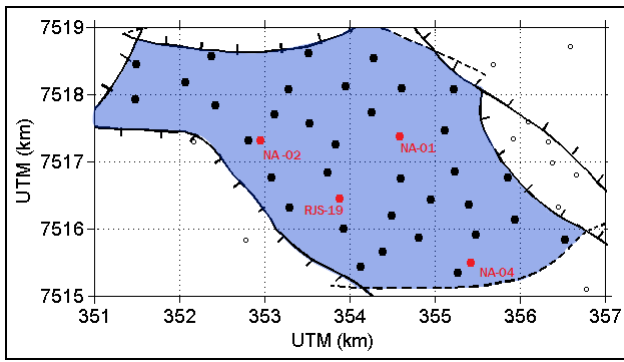


Figure 1: The Namorado field structural map. The area in blue highlights the region of interest. Black circles are the wells used in this work, while red circles represent wells containing composite logs.

2 - Calculation of Reflection Coefficient

The normal-incidence reflection coefficient or reflectivity is computed from velocity and density logs. For each interface, the reflectivity for normal incidence is given by the following equation:

$$R_{pp} = \frac{\rho_2 V_2 - \rho_1 V_1}{\rho_2 V_2 + \rho_1 V_1}, \quad (2)$$

where ρ = bulk density, V_p = P-wave velocity. The subscripts 1 and 2 indicate the values from respective logs above and below the interface. We consider that thickness of each layer is the depth sampling interval assumed during logging.

3 - Construction of Synthetic Seismograms

In this step, we simulate normal-incidence synthetic seismograms using the convolutional model. It states that a seismic trace is the result of convolving the reflectivity function of the earth with a wavelet, with or without noise added (Telford et al., 1990). Here, we ignored random noise. Thus, the following equation reads:

$$s(t) = \omega(t) * r(t), \quad (3)$$

where $s(t)$ is the synthetic seismogram, $\omega(t)$ is a wavelet and $r(t)$ represents the reflectivity log. We used the Ricker's wavelet for the simulation of synthetic seismograms, which is zero-phase wavelet with a central peak and two smaller side lobes. Further, we considered a dominant frequency of 30 Hz and temporal sampling rate of 2 ms.

4 - Maps of Seismic Amplitude

After simulating the seismic traces in all chosen wells, we followed the construction of maps of seismic amplitude at a given depth. Here, we implemented an interpolation scheme to represent spatial distribution of seismic amplitudes. According to Weber and Englund (1993), inverse distance and inverse distance squared interpolators both produce slightly better scores than ordinary and simple kriging to a larger data set. Based on previous results (Weber and Englund, 1992; Weber and Englund, 1993), the estimators defined as inverse-weighted means lead to reasonable estimations. The general interpolation formula

reads

$$x_j = \sum_{i=1}^n x_i \omega_i; \quad (4)$$

where x_j represents the estimated value in the j^{th} mesh point of the region under study and x_i represents the i^{th} sample location included in the search radius. The summation is taken over n samples included in the search area, and ω are the weights. Here we used two form for the weights. The first is defined as:

$$\omega_i = \frac{\left(\frac{1}{d_i}\right)^2}{\sum_{l=1}^{npc} \left(\frac{1}{d_l}\right)^2}, \quad (5)$$

where d_i (or d_l) is the distance between the estimation point and the i^{th} control point inside of a circular area defined *a priori* (see below). The summation npc is similar to the summation np below, which represents all samples inside in the search radius. The other weight used here is defined as:

$$\omega_i^{rs} = \frac{\left(\frac{r_s - d_i}{d_i}\right)^2}{\sum_{l=1}^{np} \left(\frac{r_s - d_l}{d_l}\right)^2}, \quad (6)$$

where r_s is the search radius. We assumed a variable search radius. This variable search radius is as 3 km at the edge of the region in Figure 1, slowing down to 1.5 km in the central region.

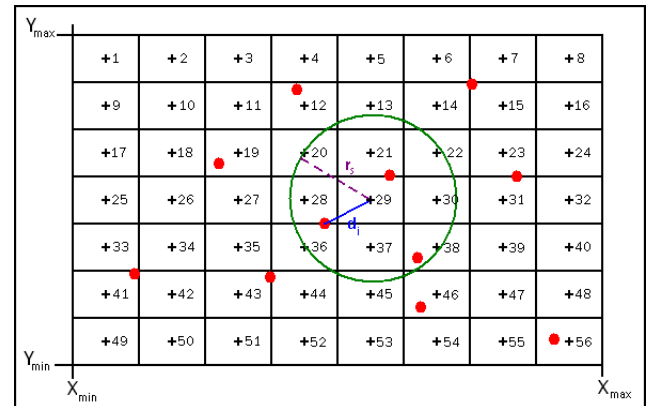


Figure 2: Illustration of the search radius scheme. The red circles are control points (i.e., well locations). In the figure, three control points will contribute to the estimation of the physical quantity for the 29th mesh point.

Results

Following the steps of the methodology described above, we simulated 39 normal-incidence synthetic seismograms, one for each chosen well. In general, the synthetic seismic traces have a good correlation with the lithology of the stratigraphic column shown in Figure 3. In well NA-02, we observe two positive high seismic amplitudes correlating with two thin layers of calcilutites around 3060 m depth. Although the wells RJS-19 and NA-04 have poor correlations, well NA-01 have an excellent correspondence of the seismic trace with the lithology. For example,

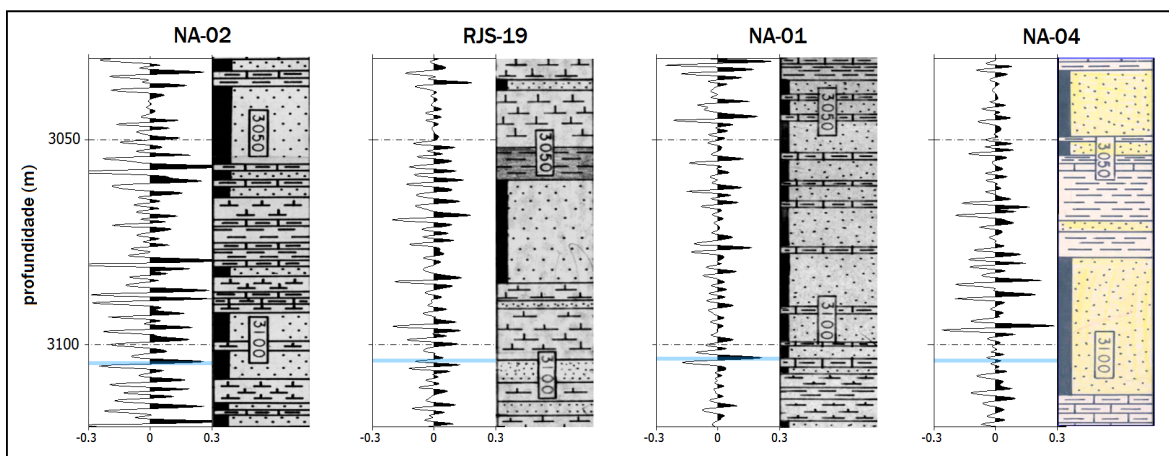


Figure 3: Synthetic seismograms with their composite logs, respectively.

the moderate positive seismic amplitude in the synthetic seismograms can be associated with the thin layers of calcilutites.

Based on the correlations between the seismic traces and their stratigraphic columns, we chose a depth for construction of the map of normal-incidence amplitudes by interpolation using the above two types of weights. We selected the depth of 3103 m for construction of the maps (see Figure 3). In this depth, we observe that wells NA-02 and NA-04 reach a productive sandstone reservoir. At well NA-01, we have the bottom of another productive sandstone reservoir as pointed out by a high, positive seismic amplitude. At well RJS-19, we notice an interface between marls and sandstones as evidenced by negative seismic amplitudes.

In Figure 4, we have the map of seismic amplitude variation using equations (4) and (5). Note that there is a trend of negative seismic amplitudes in the N-W and W-E directions. Note also that there is a concentration of positive seismic amplitudes in the central region of the Namorado field, where well NA-01 is located. Here, we can observe the bottom of the reservoir at well NA-01 along the main block of the Namorado field. These contours are more outlined in the map generated by equations (4) and (6) (see Figure 5). We also observe a concentration of positive seismic amplitudes in the SW portion and at both NW and SE extremes of the Namorado oil field.

Comparing the resulting maps, we can observe that the estimators using the weight defined by the equation (6) yields a greater correlation between the contouring levels. Table 1 and 2 show the attempt to analyze uncertainties in the maps, using some statistical measures as average value, standard deviation and minimum variance. We assessed such statistical measures as follows. First, considering only the control points (i.e., the well locations). Second, considering all locations where estimations were performed. Additionally, we considered a central region with search radius of 1.5 km. As expected Table 2 (referring to Figure 5) have little dispersion than in Table 1 (referring to Figure 4).

Discussion and Conclusions

The composite logs associated to some wells helped in the identification and qualitative interpretation of geological features in the synthetic seismograms. In this way, the interpolators based on inverse-weighted means (Weber and Englund, 1993), whose weights are described in equations (5) e (6), revealed satisfactory robustness in estimating the seismic amplitudes in the resulting maps. As the interpolation scheme, we used a variable search radius around the point where the estimation is made, favoring the interpolation with the weight described by equation (6). In this interpolation scheme, the search radius is included. Nevertheless, although the weight defined by equation (5) ignores the search radius, we believe that the interpolations with both weights provided equivalent results.

The maps of seismic amplitudes at 3103 m depth show positive amplitudes with moderate to high variation in the well NA-01, which reveals the bottom of the reservoir. However, at well NA-01 we noticed positive amplitude, suggesting an extension of the reflector defining the bottom of the reservoir. On the other hand, the directional trend of negative seismic amplitudes may be indicating the extension of the reservoir at well NA-04.

The methods used in practice for characterization of oil and gas reservoirs are mostly qualitative, but have large impact on minimizing uncertainties. Although qualitative, the interpretation of the maps representing the variation of seismic amplitudes for normal-incidence, may contribute to better understanding of the geological features in an oil and gas reservoir field. In practice, time slice are constructed from 3D seismic cubes. It is commonplace that the information generated from the interpretation of such maps have application in the study the technical viability for implementation of 4D seismic surveys in mature reservoirs. In particular, considering the Namorado reservoir, we propose that the maps of normal-incidence seismic amplitude are used for the design of multicomponent seismic lines location over the oil field. The maps of seismic amplitude generated from the processing of such data would be correlated with those constructed in this work, probably revealing hydrocarbons accumulations and areas with geological features favorable to location of producing wells.

Acknowledgments

This work was prepared in the context of master's dissertation project entitled "Maps of normal-incidence seismic amplitudes in the Namorado reservoir, Campos basin". Fabrício Augusto acknowledges a research scholarship from CAPES/Brazil for the development of his MSc dissertation in the Post-Graduation Course in Geophysics, ON-MCT. Jorge Martins acknowledges the financial support from The Brazilian Agency for the Development of Science and Technology - CNPq/Brazil (proc. no. 471647/2006-3), through the research work entitled "Caracterização de Anisotropia Sísmica Usando Perfis Geofísicos de Poços de Petróleo e Gás".

References

Augusto, F. O. A., 2009, Mapas de Amplitude Sísmica para Incidência Normal no Reservatório Namorado, Bacia de Campos, Master's dissertation, ON-MCT, Rio de Janeiro.

Augusto, F. O. A. e Martins, J. L., 2008, Relações Empíricas Não-Convencionais para Estimativa de Perfis Sônicos de Ondas Compressoriais, Rio Oil & Gas 2008 Expo and conference, Instituto Brasileiro de Petróleo, Gás e Biocombustíveis, 15-18 Setembro, Rio Centro, Rio de Janeiro, CD-ROM.

Augusto, F. O. A., Martins, J. L., and Silva, J. C., 2007, Compressional-wave velocity variation in the upper Macaé formation: A well-log regression analysis study, 10th Intern. Congress of the Braz. Geophysical Society, 19-22 November, Hotel Intercontinental, Rio de Janeiro, CD-ROM.

Dewan, J. T., 1983, Essentials of modern open-hole log interpretation, PennWell Books, 361 p.

Ellis, D. V., 1987, Well logging for earth scientists, Elsevier Science Publishing Co. Inc, 550p.

Han, D-H., Nur, A., and Morgan, D., 1986, Effects of porosity and clay content on wave velocities in sandstones: Geophysics, 51, 2093-2107.

Miller, S. L. M., and Stewart, R. R., 1990, Effects of lithology, porosity and shaliness on P- and Swave velocities from sonic logs: Canadian Journ. of Expl. Geophysics, 26, 94-103.

Tigre, C. A., and Lucchesi, C. F., 1986, Estado atual do desenvolvimento da Bacia de Campos e perspectivas. In: Seminário de Geologia de Desenvolvimento e Reservatório, DEPEX-PETROBRAS, Rio de Janeiro, 1-12. (In Portuguese).

Telford, W. M., Geldart, L. P. and Sheriff, R. E., 1990 Applied Geophysics, 2 ed. Cambridge University Press.

Vidal, A. C., Sancevero, S. S., Remacre, A. Z. e Costanzo, C. P., 2007, Modelagem Geostatística 3D da Impedância Acústica para a Caracterização do Campo de Namorado, Revista Brasileira de Geofísica, 25, no.3, 295-305.

Weber, D. D. & Englund, E. J., Evaluation and Comparison of Spatial Interpolators, Mathematical Geology 24, no.4, 1992.

Weber, D. D. & Englund, E. J., Evaluation and Comparison of Spatial Interpolators II, Mathematical Geology 24, 381-

391, 1993.

Table 1: Statistics at figure's map 4.

| Statistics | Sample | Global | Central region (R = 1.5km) |
|-----------------------------|------------------------|------------------------|----------------------------|
| Maps of Seismic Amplitude : | | | |
| Amp_{min} | -0.87×10^{-1} | -0.82×10^{-1} | -0.81×10^{-1} |
| Amp_{max} | 2.32×10^{-1} | 2.24×10^{-1} | 2.24×10^{-1} |
| Amp_{mean} | 9.84×10^{-3} | 10.76×10^{-3} | 13.67×10^{-3} |
| S_{Amp} | 6.19×10^{-2} | 3.04×10^{-2} | 3.20×10^{-2} |
| σ_{Amp} | 3.84×10^{-3} | 0.92×10^{-3} | 1.03×10^{-3} |

Table 2: Statistics at figure's map 5.

| Statistics | Sample | Global | Central region (R = 1.5km) |
|-----------------------------|------------------------|------------------------|----------------------------|
| Maps of Seismic Amplitude : | | | |
| Amp_{min} | -0.87×10^{-1} | -0.85×10^{-1} | -0.85×10^{-1} |
| Amp_{max} | 2.32×10^{-1} | 2.29×10^{-1} | 2.29×10^{-1} |
| Amp_{mean} | 9.84×10^{-3} | 11.16×10^{-3} | 15.91×10^{-3} |
| S_{Amp} | 6.19×10^{-2} | 3.88×10^{-2} | 4.23×10^{-2} |
| σ_{Amp} | 3.84×10^{-3} | 1.51×10^{-3} | 1.79×10^{-3} |

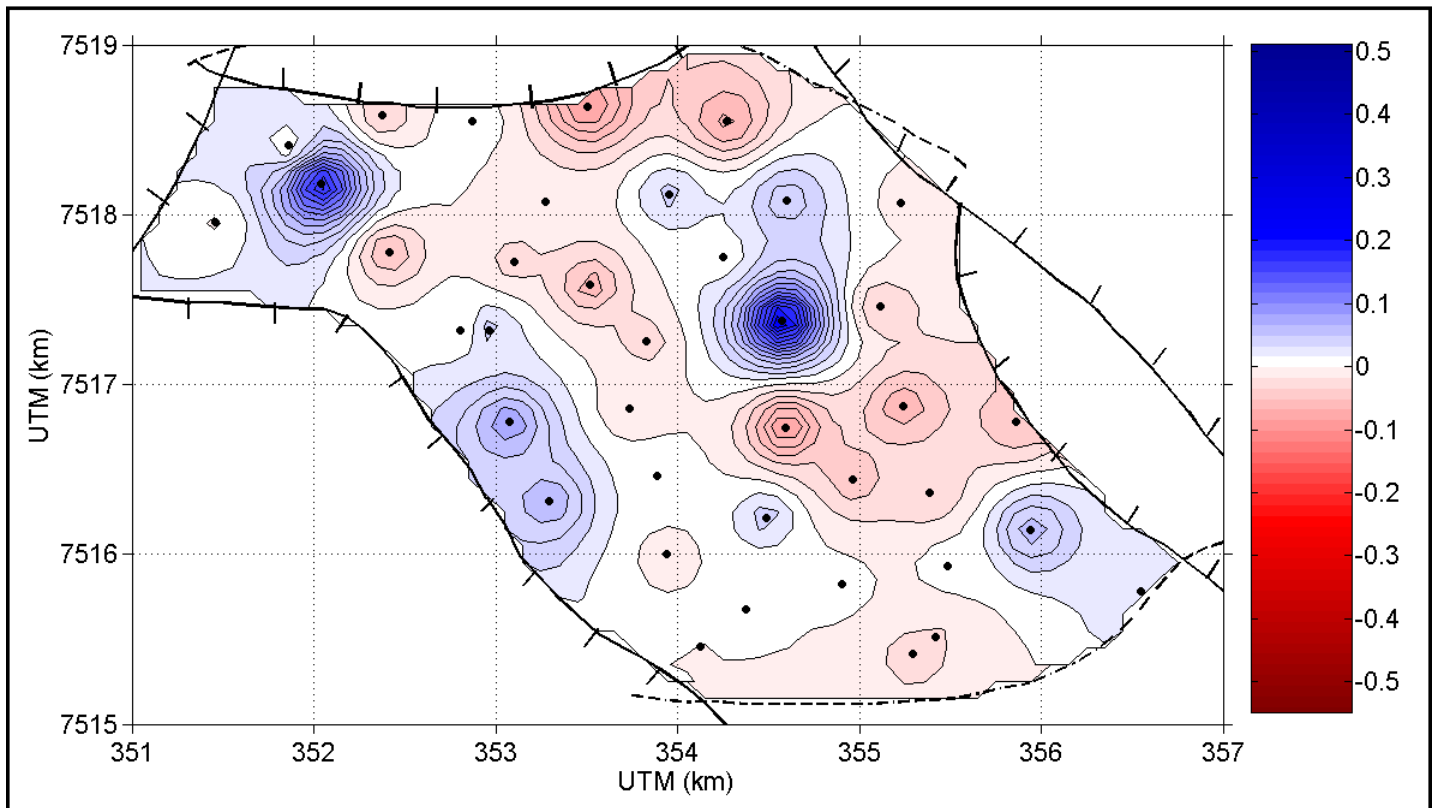


Figure 4: Map of normal-incidence seismic amplitude at 3103 m depth using weight's interpolator defined by equation (5).

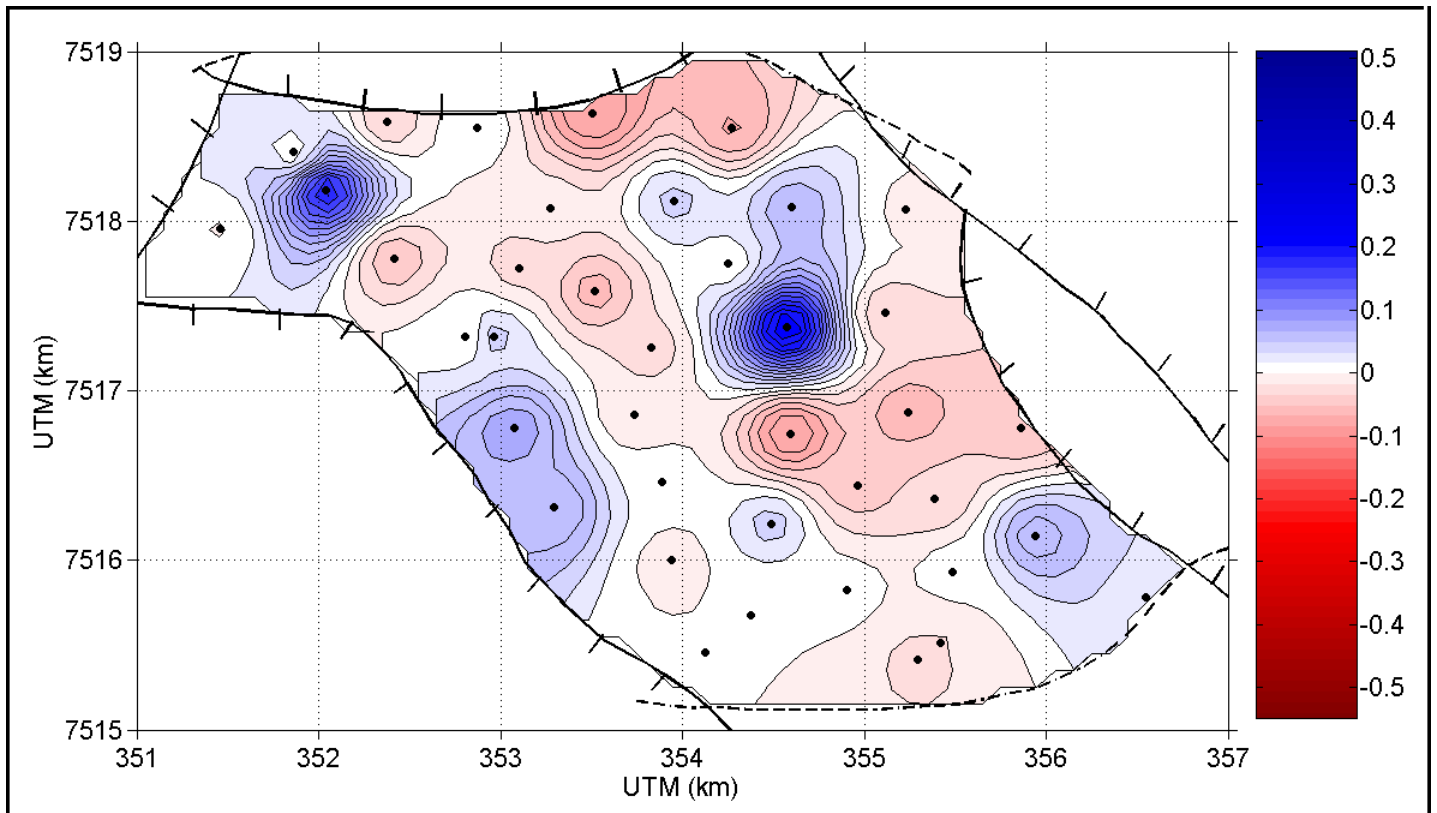


Figure 5: Map of normal-incidence seismic amplitude at 3103 m depth using weight's interpolator defined by equation (6).